International Journal of Nanomedicine

Dovepress

open access to scientific and medical research

Open Access Full Text Article

ORIGINAL RESEARCH

Bone-Targeting Peptide and RNF146 Modified Apoptotic Extracellular Vesicles Alleviate Osteoporosis

Linyuan Gui[1,*], Qingyuan Ye[2,*], Lu Yu[3], Geng Dou[1], Yang Zhou[1], Yang Liu[4], Yanqi Zhang[5], Xiaoshan Yang[1,6], Fang Jin[5], Shiyu Liu[1], Yan Jin[1], Lili Ren[1]

[1]State Key Laboratory of Oral & Maxillofacial Reconstruction and Regeneration, National Clinical Research Center for Oral Diseases, Shaanxi International Joint Research Center for Oral Diseases, Center for Tissue Engineering, School of Stomatology, The Fourth Military Medical University, Xi'an, Shaanxi, 710032, People's Republic of China; [2]State Key Laboratory of Oral & Maxillofacial Reconstruction and Regeneration, National Clinical Research Center for Oral Diseases, Shaanxi Key Laboratory of Stomatology, Digital Dentistry Center, School of Stomatology, The Fourth Military Medical University, Xi'an, Shaanxi, 710032, People's Republic of China; [3]Department of Periodontology, School and Hospital of Stomatology, Cheeloo College of Medicine, Shandong University & Shandong Key Laboratory of Oral Tissue Regeneration & Shandong Engineering Laboratory for Dental Materials and Oral Tissue Regeneration & Shandong Provincial Clinical Research Center for Oral Diseases, Jinan, Shandong, 250012, People's Republic of China; [4]Department of Anesthesiology and Perioperative Medicine, Xijing Hospital, The Fourth Military Medical University, Xi'an, Shaanxi, 710032, People's Republic of China; [5]State Key Laboratory of Oral & Maxillofacial Reconstruction and Regeneration, National Clinical Research Center for Oral Diseases, Shaanxi Clinical Research Center for Oral Diseases, Department of Orthodontics, School of Stomatology, The Fourth Military Medical University, Xi'an, Shaanxi, 710032, People's Republic of China; [6]Stomatological Hospital, School of Stomatology, Southern Medical University, Guangzhou, Guangdong, 510280, People's Republic of China

*These authors contributed equally to this work

Correspondence: Lili Ren; Yan Jin, State Key Laboratory of Oral & Maxillofacial Reconstruction and Regeneration, National Clinical Research Center for Oral Diseases, Shaanxi International Joint Research Center for Oral Diseases, Center for Tissue Engineering, School of Stomatology, The Fourth Military Medical University, Xi'an, Shaanxi, 710032, People's Republic of China, Email lanyangddgy@qq.com; yanjin@fmmu.edu.cn

Background: Osteoporosis is a highly prevalent disease that causes fractures and loss of motor function. Current drugs targeted for osteoporosis often have inevitable side effects. Bone marrow mesenchymal stem cell (BMSCs)-derived apoptotic extracellular vesicles (ApoEVs) are nanoscale extracellular vesicles, which has been shown to promote bone regeneration with low immunogenicity and high biological compatibility. However, natural ApoEVs cannot inherently target bones, and are often eliminated by macrophages in the liver and spleen. Thus, our study aimed to reconstruct ApoEVs to enhance their bone-targeting capabilities and bone-promoting function and to provide a new method for osteoporosis treatment.

Methods: We conjugated a bone-targeting peptide, $(Asp\text{-}Ser\text{-}Ser)_6$ ($(DSS)_6$), onto the surface of ApoEVs using standard carbodiimide chemistry with DSPE-PEG-COOH serving as the linker. The bone-targeting ability of $(DSS)_6$-ApoEVs was determined using an in vivo imaging system and confocal laser scanning microscopy (CLSM). We then loaded ubiquitin ligase RING finger protein146 (RNF146) into BMSCs via adenovirus transduction to obtain functional ApoEVs. The bone-promoting abilities of $(DSS)_6$-ApoEVs and $(DSS)_6$-ApoEVs^{RNF146} were measured in vitro and in vivo.

Results: Our study successfully synthesized bone-targeting and gained functional $(DSS)_6$-ApoEVs^{RNF146} and found that engineered ApoEVs could promote osteogenesis in vitro and exert significant bone-targeting and osteogenesis-promoting effects to alleviate osteoporosis in a mouse model.

Conclusion: To promote the bone-targeting ability of natural ApoEVs, we successfully synthesized engineered ApoEVs, $(DSS)_6$-ApoEVs^{RNF146} and found that they could significantly promote osteogenesis and alleviate osteoporosis compared with natural ApoEVs, which holds great promise for the treatment of osteoporosis.

Keywords: osteoporosis, mesenchymal stem cells, apoptotic extracellular vesicles, bone-targeting, bone regeneration

Received: 2 August 2023
Accepted: 16 November 2023
Published: 17 January 2024

Graphical Abstract

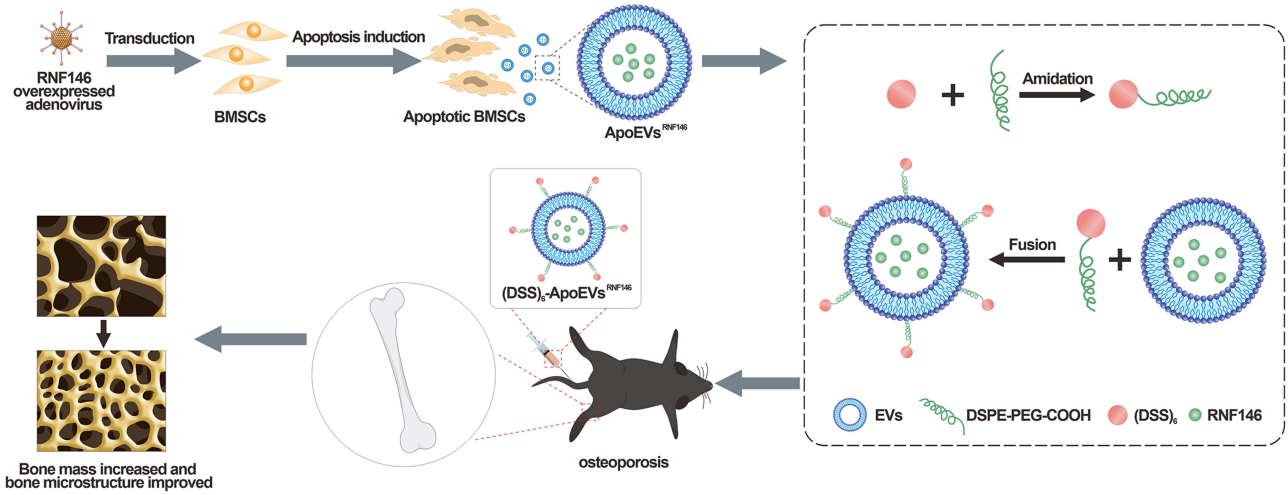

Introduction

Osteoporosis is a highly prevalent, debilitating disease of global concern, and is characterized by a high morbidity rate and severe impact on physical function. This chronic disease results in a marked reduction in bone mass, degradation of bone microstructure, and increased risk of fragility fractures.[1] Bone homeostasis is disrupted when the rate of bone resorption is faster than that of bone formation, resulting in a discontinuous trabecular bone structure and insufficient bone density.[2] Osteoporosis often affects postmenopausal women due to estrogen deficiency, manifesting as a decrease in bone mass and the risk of fracture.[3]

Current drugs used for osteoporosis treatment mainly focus on anti-bone resorption or the promotion of bone formation; however, these drugs have inevitable side effects.[4] Bisphosphonates are the most widely used bone resorption inhibitors that can suppress osteoclast activity, but their long-term use may cause medication-related osteonecrosis of the jaw (MRONJ) or gastrointestinal discomfort.[5] Supplementation with exogenous estrogens is often used for postmenopausal estrogen deficiency-induced osteoporosis; however, long-term estrogen administration has a potential risk of breast cancer, uterine cancer and endometritis.[1,6–8] Therefore, there is an urgent need to develop novel, biocompatible, and effective drugs that can target osteoporosis.

Bone marrow mesenchymal stem cells (BMSCs) have been extensively employed as promising cellular entities in the field of bone regeneration, owing to their robust self-renewal capacity and multifaceted differentiation potential.[9] Previous studies have shown that the vast majority of transplanted BMSCs would undergo apoptosis within the first few days after transplantation, mainly due to ischemia, inflammation and microenvironmental changes.[10,11] During apoptosis, a cascade of events results in the formation and release of nanoscale membrane-wrapped structures called apoptotic extracellular vesicles (ApoEVs).[12]

ApoEVs are a major subtype of extracellular vesicles based on their biogenesis and size, which are generally 0.1–5 μm in diameter. The larger ApoEVs were categorized as apoptotic bodies (1–5 μm in diameter), whereas the smaller ApoEVs were described as apoptotic microvesicles (0.1–1 μm in diameter).[13,14] ApoEVs are not just debris but are implicated in the transfer, recycling, and reuse of materials in cells.[15,16] With the advancement of regenerative medicine, ApoEVs have emerged as a promising therapeutic option for osteoporosis treatment due to their low immunogenicity and high biological compatibility. Increasing evidence suggests that apoptosis plays a crucial role in initiating regeneration and immune regulation.[17] Previous investigations have demonstrated that ApoEVs derived from MSCs can rescue MSCs impairment and mitigate osteopenia in various models by activating the Wnt/β-catenin pathway.[18] Furthermore, MSCs derived ApoEVs have been shown to facilitate the proliferation, migration, and differentiation of endogenous BMSCs by

augmenting intracellular reactive oxygen species (ROS) levels and subsequently activating JNK signaling, thereby promoting the repair of calvaria defects.[19] In terms of angiogenesis, MSCs-derived ApoEVs can stimulate vascular regeneration by inducing the production of CXCL12 to counteract apoptosis and recruit endothelial progenitor cells.[20] Additionally, ApoEVs derived from SHED (Stem cells from human exfoliated deciduous teeth) can increase the expression of genes related to angiogenesis after uptake by endothelial cells and subsequently promote pulp vascular reconstruction through increasing autophagy level.[21]

However, natural ApoEVs do not possess satisfactory bone targeting capacity, which greatly limits their clinical application. Therefore, the development of engineered ApoEVs with bone-targeting functions is of great significance. In this study, we designed and synthesized a kind of rearranged extracellular vesicle $(Asp\text{-}Ser\text{-}Ser)_6$-$ApoEVs^{RNF146}$ (also named by $(DSS)_6$-$ApoEVs^{RNF146}$) to improve both bone targeting and osteogenesis promoting function of natural ApoEVs. The dual modification of the membrane surface and storage of natural vesicles could provide a triple intervention treatment for osteoporosis. Our strategy would provide a new therapeutic method for osteoporosis and an important theoretical and experimental basis for treating bone diseases such as osteoporosis.

Materials and Methods

Materials

Bone-targeting peptides $(DSS)_6$ and Rhd-$(DSS)_6$ (99% purity) were synthesized by Yaguang Peptide Biotechnology (China). DSPE-PEG-COOH (PG2-CADS-2K) was purchased from NANOCS (USA). EDC (CAS:25952-53-8) and NHS (CAS:6066-82-6) were purchased from Sigma–Aldrich (USA). Osteogenic induction medium (CTCC-Y001) was purchased from CTCC Biosciences (China). The BCIP/NBT Alkaline Phosphatase (ALP) Color Development Kit was purchased from Beyotime Biotechnology (China). The Alizarin Red S dye solution was purchased from Servicebio (China). Staurosporine (9953S), Anti-RUNX2 (D1H7) antibody were purchased from Cell Signaling Technology (USA). Anti-ALP (ab203106) antibody was purchased from Abcam (USA). Mouse RING finger protein146 (RNF146) gene overexpressed adenovirus (HH20220401XAZC-AD01) and a negative control were designed and synthesized by Hanbio Biotechnology (China). Decalcified 17% EDTA solution (pH 7.2) was purchased from Proandy (China). Mouse TNF-α and IL-6 ELISA kits were purchased from Neobioscience (China).

Animals

All animal experiments were approved and performed in accordance with the guidelines of the Animal Care Committee of Fourth Military Medical University. Eight-week-old female C57BL/6 mice were used to establish the osteoporosis model. Four-week-old female wild-type C57BL/6 mice were used to isolate BMSCs and induce apoptosis to obtain ApoEVs.

Extraction and Characterization of ApoEVs

Isolation of BMSCs and extraction of BMSCs derived ApoEVs were performed as described in our previous work.[22] The BMSCs were treated with staurosporine (0.5 μM) for 6 h to induce apoptosis. Then, cell culture medium was collected and centrifuged at 800 g for 10 min to discard the dead cells, impurities, and other pellet. The supernatant was centrifuged at 16,000 g for 30 min at 4°C. After repeating this twice, the supernatants were removed and ApoEVs pellets were resuspended in 1×PBS, stored at −80°C for subsequent experiments. The size of ApoEVs was monitored by Dynamic Light Scattering (DLS) (ZSE, Malvern, UK). The morphology of ApoEVs was observed using transmission electron microscopy (TEM) (Hitachi, Japan). The solution containing ApoEVs was applied to a copper grid coated with carbon membrane and air-dried. Negative staining was performed with 2% phosphotungstic acid. Samples were observed at an acceleration voltage of 75 kV.

Flow cytometry (FC) and Western blotting were performed to characterize specific ApoEVs markers. Annexin V-FITC staining was conducted using an Annexin V-FITC/PI apoptosis assay kit (eBioscience, BMS500FI-300/300T) following the manufacturer's protocol. Specifically, ApoEVs were collected, resuspended in 100 μL of 1×binding buffer, and stained with 5 μL FITC-labeled Annexin V for 15 min. The stained ApoEVs were analyzed using FC (Beckman-Coulter, CytoFLEX) and confocal laser scanning microscope (CLSM) (Nikon, Japan). Specific ApoEVs protein levels were determined by Western blotting.

Synthesis of DSPE-PEG-$(DSS)_6$

$DSPE\text{-}PEG\text{-}(DSS)_6$ was synthesized by conjugation of $(DSS)_6$ and DSPE-PEG-COOH via an amidation reaction. DSPE-PEG-COOH (18 mg) was dissolved in distilled water and EDC (61.2 mg) and NHS (37.2 mg) were used to catalyze the reaction for half an hour. $(DSS)_6$ (12 mg) was added to the reaction system and rotated for 10 h in the dark. The uncoupled molecules were removed by overnight dialysis (molecular weight cut-off of 3000 Da) (YOBIOS, YD20DG28). $DSPE\text{-}PEG\text{-}(DSS)_6$ was freeze-dried and the powder was stored at −20 °C until use. Fourier-transform infrared spectroscopy (FTIR, Thermo Scientific Nicolet iS2, USA) and high-resolution mass spectroscopy (HRMS, Thermo Scientific Q Exactive, USA) were used to identify the correct compound.

Preparation and Characterization of $(DSS)_6$-ApoEVs

$DSPE\text{-}PEG\text{-}(DSS)_6$ and the desired amount of ApoEVs were incubated for 2 h with rotation at 37 °C in the dark, followed by centrifugation at 16,000 g for 30 min to obtain $(DSS)_6$-ApoEVs compounds. The characterization of $(DSS)_6$-ApoEVs was based on the characterization of ApoEVs.

In vivo Fluorescence Imaging

ApoEVs were collected and resuspended in the DiR dye (5 μM) (Invitrogen, D12731). After 15 min, $(DSS)_6$-ApoEVs were injected into the mice through the tail vein for distribution analysis, while natural ApoEVs were also injected as control. Three hours later, the mice were euthanized, and the tissues were excised and examined using an in vivo imaging system (Caliper Life Science, IVIS Lumina II). Fluorescence in the femurs was measured and analyzed using Living Image software.

To further quantify the targeting efficiency, ApoEVs were labeled by DiD dye (5 μM) (Yeasen, 40758ES25) and then resuspended in DiD solution for 30 min in the dark. The same doses of ApoEVs-DiD (use as control group) and $(DSS)_6$-ApoEVs-DiD were injected into the mice through the tail vein, while PBS was also injected as blank control. Femurs were harvested and fixed to obtain frozen sections. CLSM was used to observe the distribution of ApoEVs.

Safety Evaluation of $(DSS)_6$-ApoEVs In vivo

Mice were intravenously injected with PBS (blank control group), natural ApoEVs (control group), and $(DSS)_6$-ApoEVs (the amount of ApoEVs is 300 μg). After 24 h, the blood samples were collected and centrifuged twice at 4000 rpm for 10 min. The serum concentrations of IL-6 and TNF-α were measured using ELISA. Serum alanine transaminase (ALT), aspartate aminotransferase (AST), creatine kinase (CK), creatinine (CR), and blood urea nitrogen (BUN) levels were measured using diagnostic kits (Changchun Huili).

The organs were excised and stained with hematoxylin and eosin (H&E) staining. Paraformaldehyde-fixed tissues (4%) were dehydrated using a graded ethanol series. The samples were then embedded in paraffin and cut into 4 μm-thick sections. H&E staining was performed to evaluate organ toxicity of $(DSS)_6$-ApoEVs.

Internalization of ApoEVs into BMSCs In vitro

Rhodamine-labeled ApoEVs were obtained by modifying rhodamine-labeled $(DSS)_6$ onto the surface of ApoEVs, PKH26-labeled ApoEVs were obtained by pre-labeling with the PKH26 Red Fluorescent Cell Linker Kit (Sigma, MINI26) according to the manufacturer's instructions.

The BMSCs (P2) were plated on confocal dishes and maintained in a cell incubator. When the cells reached 50–60% confluence, ApoEVs labeled with Rhodamine or PKH26 red fluorescence were added to the BMSCs at a concentration of 10 μg/mL for 12 h. After fixation with 4% paraformaldehyde, cells were stained with fluorescein isothiocyanate-phalloidin (FITC-Phalloidin) (Yeasen, 40735ES75) and cell nuclei staining solution (Hoechst 33342) (Sigma, 14533). Fluorescence was observed using CLSM.

ALP and Alizarin Red Staining Experiment

Different types of ApoEVs (natural ApoEVs, $(DSS)_6$-ApoEVs, and RNF146 modified ApoEVs) were used to treat OVX mice derived BMSCs to determine whether they could induce osteogenic differentiation. After osteogenic induction for 7 days ALP staining and 28 days Alizarin red staining were performed respectively according to the manufacturer's protocol. Briefly, for ALP staining, after discarding the medium in the culture plate, wash it twice with PBS, and then add 4% paraformaldehyde for 30 min at room temperature. Then wash it with PBS for twice again, followed by adding BCIP/NBT dyeing solution and incubating it for 15 min to anticipated coloring in the dark. The BCIP/NBT dyeing solution is a mixture of 10 mL buffer, 33 μL BCIP solution (300×), and 66 μL NBT solution (150×). For Alizarin red staining, after discarding the medium in the culture plate, wash it twice with PBS, and then add 60% isopropyl alcohol for 30 min at room temperature. Then wash it with PBS for twice again, followed by adding alizarin red dye for about 1 min, and then photographed after washing with ddH_2O. Finally, the intensity of ALP staining was measured using ImageJ software, while quantitative analysis of alizarin red staining was performed using 10% cetylpyridinium chloride to dissolve the stain, and the absorbance at 540 nm was measured using an enzymatic immunoassay.

Western Blot Analysis

Western blot analysis was conducted 7 days after osteogenesis induction to verify the expression of osteogenic-related proteins. Protein samples from different groups of cells (normal BMSCs, OVX mice derived BMSCs, and OVX mice derived BMSCs treated with $(DSS)_6$-ApoEVs) were extracted using RIPA buffer (Beyotime Biotechnology, P0013) containing protease inhibitors (Roche, 04693132001). The protein concentration was quantified using a BCA Protein assay kit (Beyotime Biotechnology, P0012). Denatured proteins from all samples were prepared at a final concentration of 1 mg/mL, separated by SDS-PAGE, and transferred to polyvinylidene difluoride (PVDF) membranes (Roche, 03010040001) in a Bio-Rad Electrophoresis System. Membranes were blocked with 5% bovine serum albumin (BSA) solution (DIYIBio, DY60105) and incubated with primary antibodies (anti-RUNX2, anti-ALP, or anti-β-actin) for 12 h at 4°C, followed by incubation with the corresponding secondary antibodies for 1 h, and visualization with an imaging system (Tanon 5500, Shanghai).

BMSCs Transfection and Isolation of RNF146-Overexpressed ApoEVs

To upregulate the expression of RNF146 in ApoEVs, a specific adenovirus (HH20220401XAZC-AD01) containing enhanced green fluorescent protein (EGFP) and stably overexpressed RNF146 was used to transduce cells after screening for a suitable multiplicity of infection (MOI). BMSCs (P2) were seeded onto confocal dishes and then attached to 50% confluence, and adenovirus and negative controls were used to transduce the cells. After 2 days, the green fluorescence expressed in BMSCs was observed using CLSM to detect efficiency. BMSCs were incubated with staurosporine to obtain RNF146-overexpressed ApoEVs at 36–48 hours after transfection.

Establishment of Mice Osteoporosis Model and Evaluation of Therapeutic Effect

Eight-week-old female C57BL/6 mice were subjected to bilateral sham or ovariectomy (OVX) using a dorsal approach. The mice were anesthetized with an intraperitoneal injection of sodium pentobarbital. The skin around the midline of the back was then shaved and disinfected. Linear incisions were made bilaterally on the skin along the lumbar vertebrae to expose ovaries. Then, the bilateral ovaries and fat tissues were gently removed from mice to establish the osteoporosis model, while the mice in the control group only had some adipose tissue around the ovary removed as a control. Finally, the tissues were repositioned, and the muscle tissue and skin were sutured carefully.

To investigate the potential application of different types of ApoEVs in osteoporosis therapy, the mice were randomly separated into groups to receive PBS or different types of ApoEVs via tail vein injection from the fourth week after OVX surgery, while normal C57 mice were used as normal control. The therapeutic dose was 10 mg/kg once a week for four weeks. Micro-computed tomography (micro-CT) analysis (μCT; AX-2000, Always Imaging, China) was used to evaluate therapeutic effects. The femoral samples were scanned beginning at 1 to 1.5 mm away from the growth plates and extending along the femur diaphysis to the proximal direction for 50 continuous slices of about 1 mm at a resolution of

5.2 μm, After 3D image reconstruction, the bone mineral density (BMD), bone volume over tissue volume (BV/TV), trabecular number (Tb. N), trabecular thickness (Tb. Th), bone surface/bone volume (BS/BV), and trabecular separation (Tb. Sp) were obtained to evaluate new bone formation using auxiliary software (VG Studio MAX 3.5).

Statistical Analysis

Data are presented as the mean ± SD. Data distribution was tested using the Shapiro–Wilk test. For normally distributed data, Student's *t*-test (two-tailed) and one-way analysis of variance (ANOVA) were performed to compare two groups and multiple group comparisons, respectively. Tukey's multiple comparison test was used to determine the significance between groups after one-way ANOVA. When data were abnormally distributed, the Mann–Whitney and Kruskal–Wallis tests were performed. P values were considered statistically significant at $P < 0.05$. Statistical analyses and graphs were generated using GraphPad Prism8.02 (GraphPad Software, USA).

Results

Synthesis and Characterization of $(DSS)_6$-ApoEVs

Natural ApoEVs were isolated from the culture supernatants of apoptotic mBMSCs by differential centrifugation after induction of apoptosis by staurosporine. Based on phosphatidylserine exposure on the ApoEVs plasma membrane, FC and CLSM showed that more than 90% of ApoEVs were Annexin V-positive (Figure S1A and B). Western blot analysis showed that the isolated ApoEVs expressed the specific marker cleaved caspase-3 (Figure S1C).

To enhance the bone-targeting ability of ApoEVs, bone-targeting peptide $(DSS)_6$ was modified on the membrane surface of ApoEVs. DSPE-PEG-COOH (MW:2781.42) and $(DSS)_6$ (MW:1866.6447) were conjugated by loss of H_2O (MW:18.0153) to obtain the final compound DSPE-PEG-$(DSS)_6$. The modified product, DSPE-PEG-$(DSS)_6$, had typical cleavage peaks of the polymer with a MW of 2313.3058, which coincides with the theoretical MW of 2313.5162 (Figure 1A). FTIR spectra provided supportive evidence that $(DSS)_6$ was conjugated to DSPE-PEG-COOH. The characteristic bands of the peptide at 3289 and 1632cm^{-1} were present in pure $(DSS)_6$ and $(DSS)_6$-bound lipids. Characteristic bands of PEG were also observed at 2918, 2887, 1112cm^{-1} in both DSPE-PEG-COOH and DSPE-PEG-$(DSS)_6$ (Figure 1B). The HRMS and FTIR results showed that an amidation reaction occurred between $(DSS)_6$ and DSPE-PEG-COOH.

To confirm that $(DSS)_6$ was successfully conjugated with ApoEVs membranes, $(DSS)_6$ was labeled with rhodamine to form Rhd-$(DSS)_6$. The FC results showed that the ApoEVs conjugated with $(DSS)_6$ showed a strong red fluorescence signal, which accounted for approximately 48% (Figure 1C). ApoEVs were labeled with PKH67 using the PKH67 Green Fluorescent Cell Linker Kit (Sigma, MINI67), after reacting with Rhd-$(DSS)_6$, the co-localization of Rhd-$(DSS)_6$ and $ApoEVs^{PKH67}$ was observed by CLSM, indicating that Rhd-$(DSS)_6$ successfully bound to the ApoEVs membrane (Figure 1D). DLS showed that the average diameter of $(DSS)_6$-ApoEVs was 220–396 nm, which was not significantly different from that of the naked ApoEVs (average diameter 220–342 nm) (Figure 1E). Transmission electron microscopy (TEM) was used to confirm the size measured by DLS. The morphology of the $(DSS)_6$-ApoEVs, which were spherical and intact, was also observed using TEM (Figure 1F). These results showed that $(DSS)_6$ can be successfully modified onto the surface of ApoEVs by inserting a "phospholipid tag" DSPE-PEG-COOH, into the lipid membrane of ApoEVs. The modified $(DSS)_6$-ApoEVs maintained their size and shape.

Evaluation of the Bone Targeting Ability of $(DSS)_6$-ApoEVs

Subsequently, the bone-targeting ability of the $(DSS)_6$-ApoEVs was tested in vivo. Three hours after DiR-labeled $(DSS)_6$-ApoEVs were intravenously injected into the mice, bone samples were collected for testing. Ex vivo fluorescence imaging showed that the amount of $(DSS)_6$-ApoEVs accumulated in the bone was significantly higher than that of the ApoEVs (Figure 2A and B). Frozen sections under CLSM showed that the DiD fluorescence distribution of the femur in the $(DSS)_6$-ApoEVs-DiD group was significantly greater than that in the ApoEVs-DiD group (Figure 2C and D). These results showed that $(DSS)_6$ modified ApoEVs could enhance bone-targeting ability.

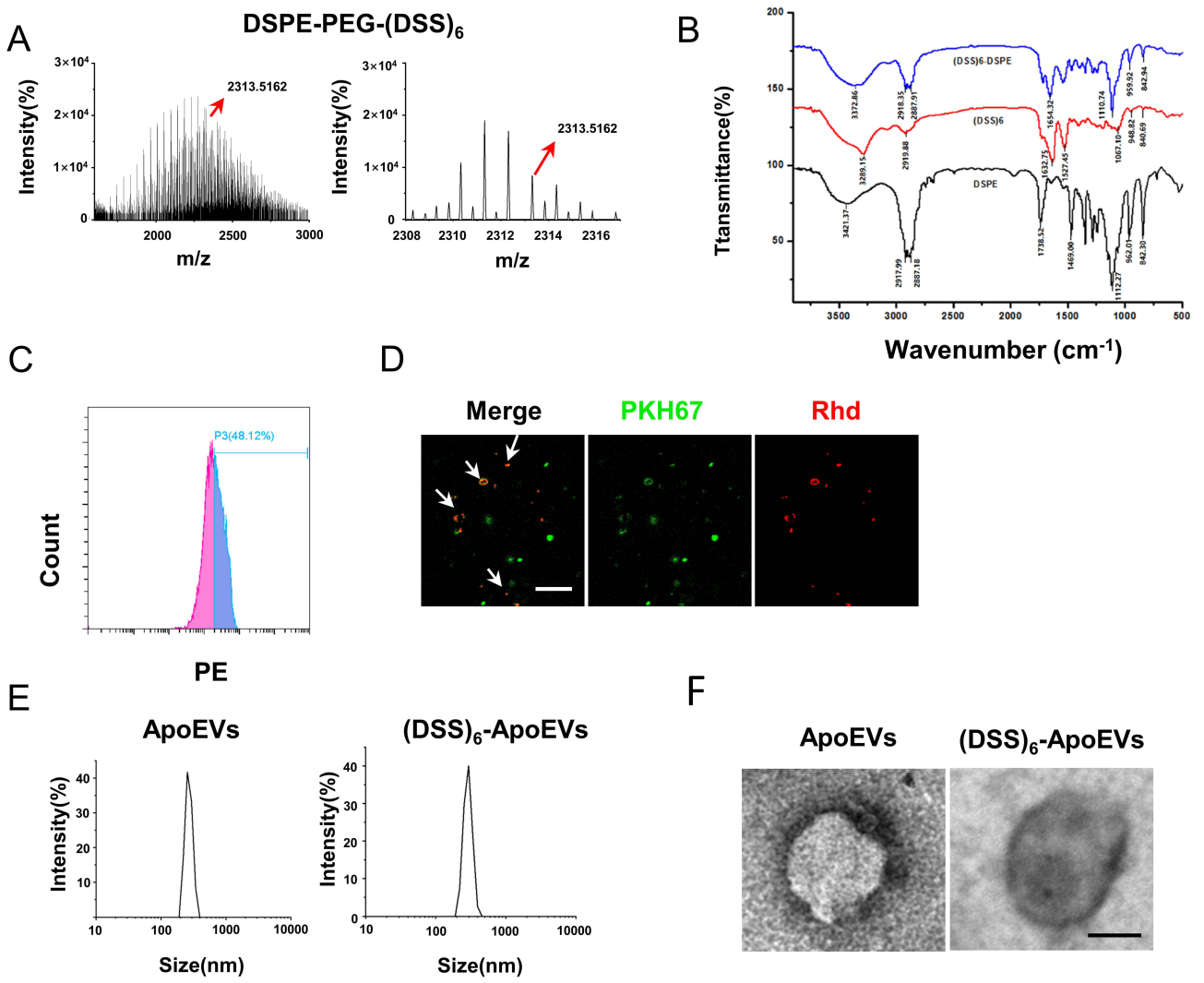

Figure 1 Characterization of $(DSS)_6$-ApoEVs. (**A**) ESI-HRMS analysis of the $(DSS)_6$ conjugation with DSPE-PEG-COOH. (**B**) FTIR analysis of the $(DSS)_6$ conjugation with DSPE-PEG-COOH via amidation reaction. (**C**) Flow cytometry showed the Rhd-$(DSS)_6$-ApoEVs had strong red fluorescence signal, with an insertion rate of ~48%. (**D**) Representative confocal laser scanning microscopy image showed the co-localization of Rhd-$(DSS)_6$ (red) with $ApoEVs^{PKH67}$ (green), indicated that $(DSS)_6$ could insert into the membrane of ApoEVs. Scale bar, 10 μm. (**E**) Size distribution of ApoEVs and $(DSS)_6$-ApoEVs analyzed by DLS. (**F**) Representative TEM image of ApoEVs and $(DSS)_6$-ApoEVs, showed intact spherical structure. Scale bar, 200 nm.

The Biosafety of $(DSS)_6$-ApoEVs

To determine the safety of $(DSS)_6$-ApoEVs in vivo, tissues (the heart, liver, spleen, lungs, and kidneys) were collected for histopathological examination. No obvious tissue damage was observed by H&E staining (Figure 3A). Serum levels of ALT, AST, CK, CR, and BUN were measured to assess liver, heart, and kidney function. No significant difference was observed between the $(DSS)_6$-ApoEVs group and PBS groups (Figure 3B). $(DSS)_6$-ApoEVs did not cause an increase in the serum levels of IL-6 and TNF-α (Figure 3C), indicating that there were no evident immune responses caused by $(DSS)_6$-ApoEVs. The body weight of each group of mice was also recorded; the $(DSS)_6$-ApoEVs group showed no significant difference compared with the control or ApoEVs groups but was slightly lighter than that of the OVX group with statistical difference (Figure 3D). These results indicated that $(DSS)_6$-ApoEVs are safe for in vivo applications.

Biological Function of $(DSS)_6$-ApoEVs In vitro

We determined whether $(DSS)_6$-ApoEVs regulate the biological functions of BMSCs. First, mBMSCs were incubated with $(DSS)_6$-ApoEVs to determine whether recipient BMSCs engulfed $(DSS)_6$-ApoEVs. After treatment with $(DSS)_6$-ApoEVs for 24 h, compared with natural ApoEVs (Figure S1D), Rhodamine-labeled exogenous $(DSS)_6$-ApoEVs were

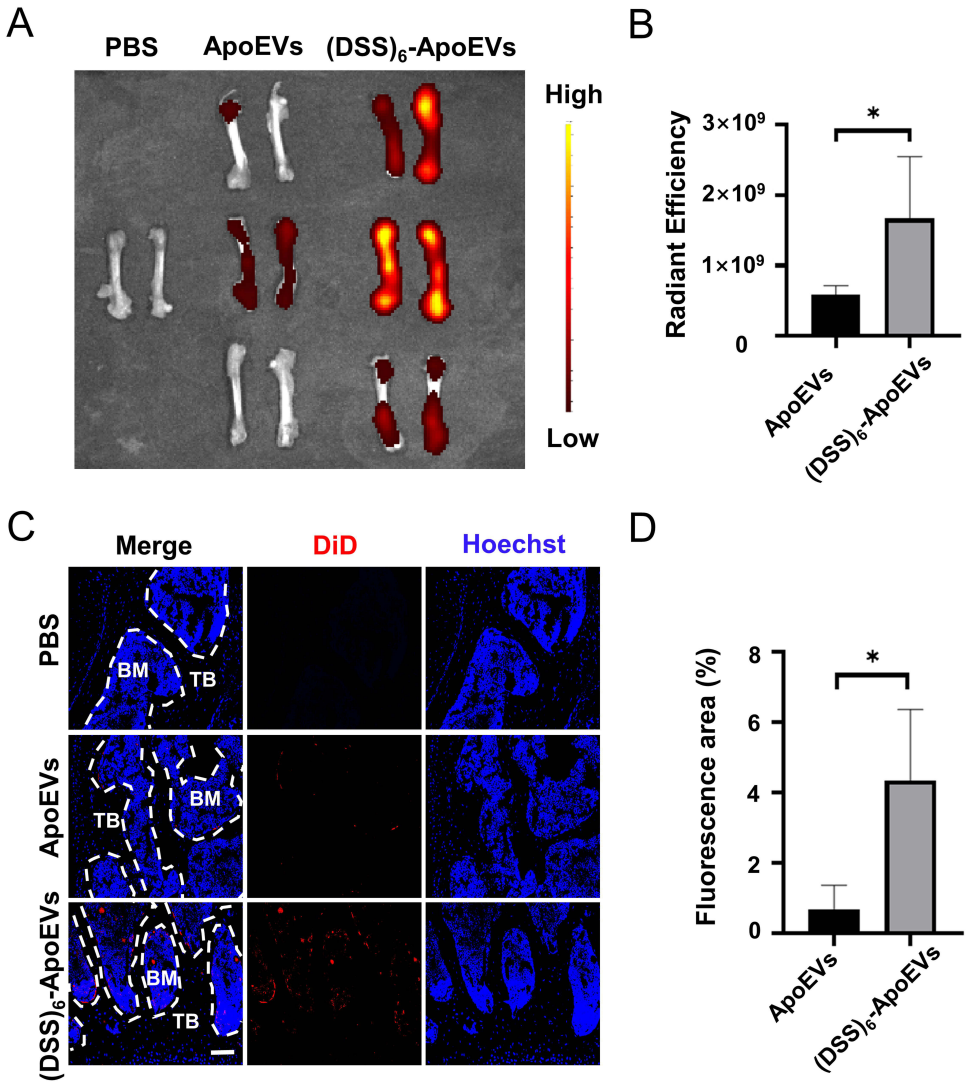

Figure 2 Evaluation of bone targeting ability of $(DSS)_6$-ApoEVs. (**A**) In vivo fluorescence distribution of DiR-labeled ApoEVs and $(DSS)_6$-ApoEVs in mouse femurs after injection. (**B**) Quantitative analysis of the fluorescence intensity in mouse femurs (n = 6). (**C**) Representative fluorescent images of DiD-labeled ApoEVs and $(DSS)_6$-ApoEVs in frozen femur sections observed by CLSM. Scale bar, 100 μm. (**D**) Quantitative fluorescence analysis of positively stained ApoEVs targeted to the bone region was performed using ImageJ software (n = 3). *$P < 0.05$.
Abbreviations: DiR, iodide [1,1-dioctadecyl-3,3,3,3-tetramethylindotricarbocyanine iodide]; DiD, 1,1′-dioctadecyl-3,3,3′,3′-tetramethylindodicarbocyanine perchlorate.

engulfed by phalloidin-labeled mBMSCs, mainly around the nucleus (Figure 4A), suggesting that $(DSS)_6$-ApoEVs can be engulfed by BMSCs.

$(DSS)_6$-ApoEVs were then added to the medium during osteogenic induction to verify the effect of $(DSS)_6$-ApoEVs on the osteogenic differentiation of BMSCs. ALP is an important indicator for detecting the osteogenic differentiation of BMSCs, whereas Alizarin red staining showed mineralized nodule formation. After osteogenic induction for 7 and 28 days, ALP (Figure 4B) and alizarin red staining (Figure 4C) of the calcium nodules were performed, respectively. The results showed that the osteogenic differentiation ability of OVX-BMSCs treated with $(DSS)_6$-ApoEVs was significantly higher than that of the OVX group. The expression of the osteogenic markers ALP and runt-related transcription factor 2 (RUNX2) in mice treated with $(DSS)_6$-ApoEVs was remarkably increased compared to that in the OVX group (Figure 4D). These results indicated that $(DSS)_6$-ApoEVs enhanced the osteogenic differentiation of BMSCs.

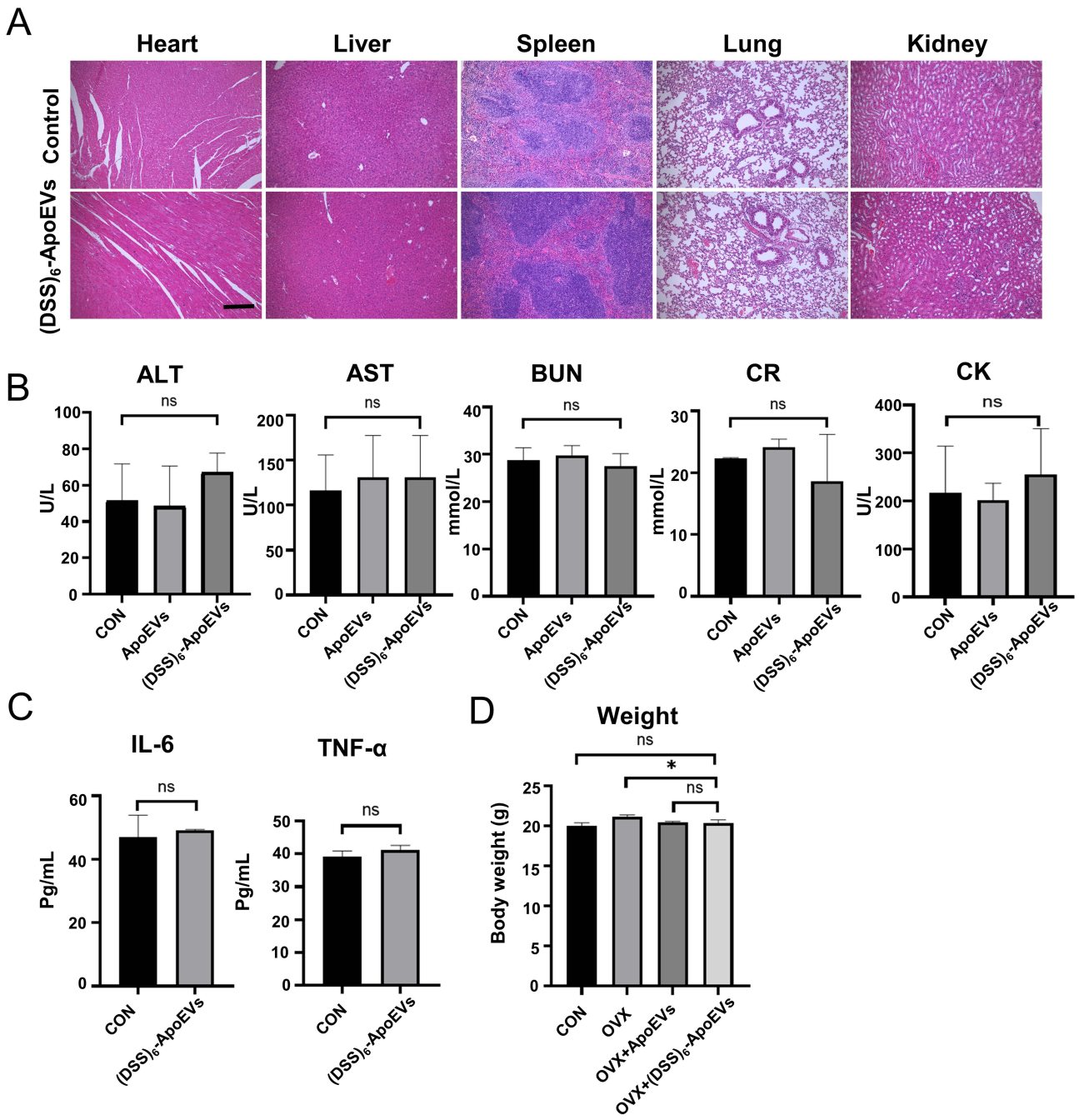

Figure 3 Evaluation of biocompatibility of $(DSS)_6$-ApoEVs in vivo. (**A**) H&E staining images of organs from PBS-treated-and $(DSS)_6$-ApoEVs-treated groups. Scale bar, 100 μm. (**B**) Levels of serum ALT, AST, BUN, CR, and CK in the PBS-treated, ApoEVs-treated, and $(DSS)_6$-ApoEVs-treated groups. All values were within the normal range (ALT: 10.06–96.47 U/L; AST: 36.31–235.48 U/L; BUN:10.81–34.74 mmol/L; CR:10.91–85.09 μmol/L; CK:0–2070.55 U/L). (**C**) Serum TNF-α and IL-6 levels were measured by ELISA. (n = 3). (**D**) Body weights of mice in different groups (n = 4). *$P < 0.05$.

Abbreviations: NS, not significant; CON, control; ALT, Alanine transaminase; AST, Aspartate aminotransferase; CK, creatine kinase; BUN, blood urea nitrogen; CR, creatinine.

Anti-Osteoporotic Effects of $(DSS)_6$-ApoEVs In vivo

After confirming the enhancement of osteogenic differentiation of BMSCs caused by $(DSS)_6$-ApoEVs in vitro, the effects of $(DSS)_6$-ApoEVs in osteoporosis treatment in vivo were explored (Figure 5A). Micro-CT results showed that $(DSS)_6$-ApoEVs increased bone mass in OVX mice compared to that in the ApoEVs group (Figure 5B), which was also emphasized by the quantities of BMD and BV/TV (Figure 5C and D). Moreover, the bone microstructure parameters in the distal femora, such as Tb. N and Tb. Th, were increased, whereas BS/BV and Tb. Sp were significantly decreased in

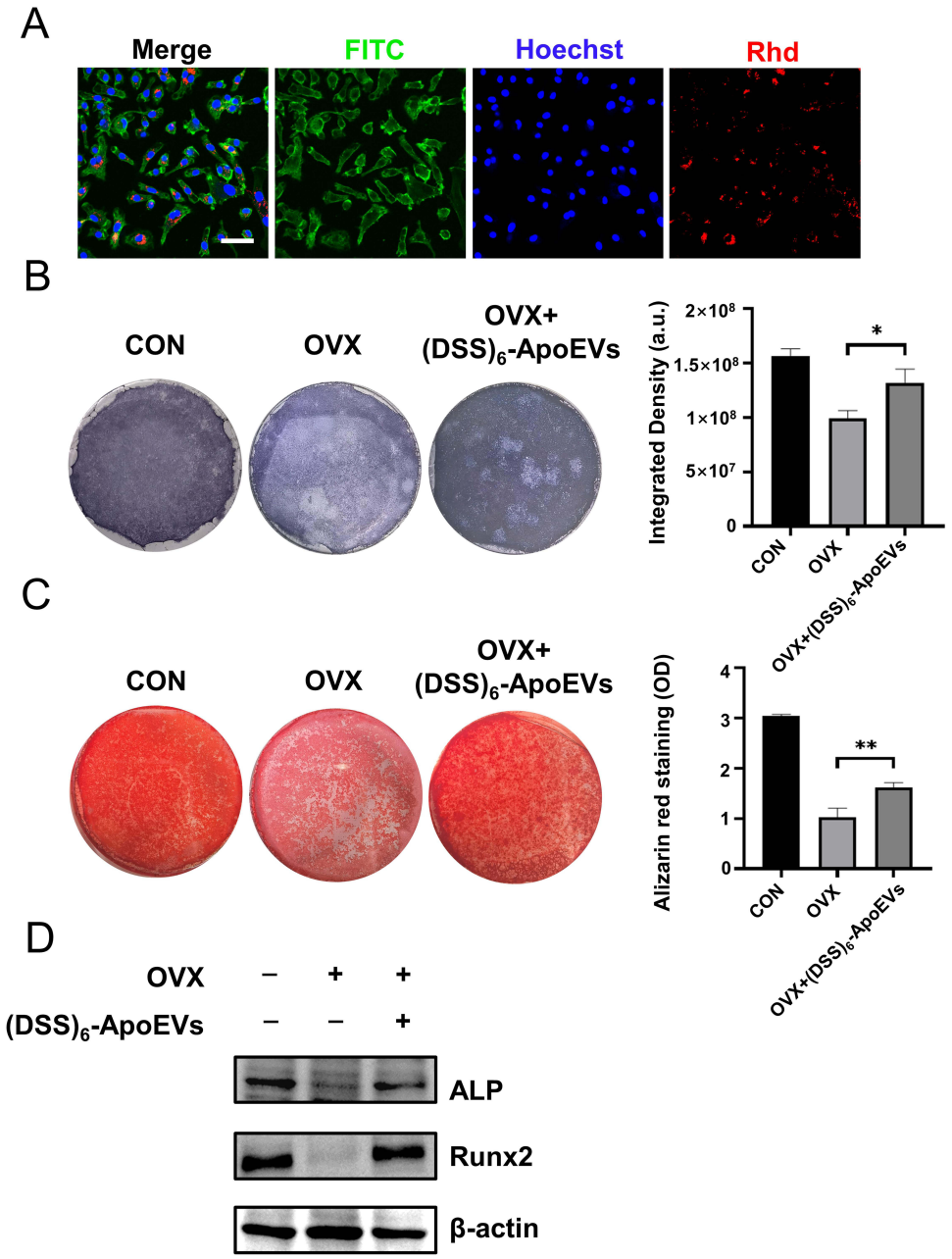

Figure 4 Antiosteoporosis efficacy of $(DSS)_6$-ApoEVs in vitro. (**A**) Representative images of $(DSS)_6$-ApoEVs taken up by BMSCs observed by CLSM. Red, Rhodamine-labeled $(DSS)_6$-ApoEVs; green, phalloidin labeled cytoskeleton; blue, Hoechst labeled nucleus. Scale bar, 50 μm. (**B**) ALP staining showed ALP activity of BMSCs treated by $(DSS)_6$-ApoEVs after osteogenic induction for 7 days. Quantitative analysis of ALP staining was measured by ImageJ software (n = 3). (**C**) Alizarin red staining of calcium nodules showed mineralized nodule formation of BMSCs treated by $(DSS)_6$-ApoEVs after osteogenic induction 28 days. Quantitative analysis of Alizarin red staining was conducted by the measurement of absorbance at 540 nm (n = 3). (**D**) Western blot analysis showing the expression of ALP and RUNX2 of BMSCs treated with $(DSS)_6$-ApoEVs. *$P < 0.05$, **$P < 0.01$.

$(DSS)_6$-ApoEVs group post-treatment. However, there were no significant differences in Tb. Th and BS/BV between the $(DSS)_6$-ApoEVs and ApoEVs groups (Figure 5E). These results suggested that $(DSS)_6$-ApoEVs promote osteogenesis under osteoporotic conditions.

Biological Function of $ApoEVs^{RNF146}$ In vitro

To obtain ApoEVs enriched with RNF146, HBAD-EGFP adenovirus carrying RNF146 was used to transfect BMSCs with the MOI of 100, which is appropriate for high expression of the target protein and acceptable toxicity to cells

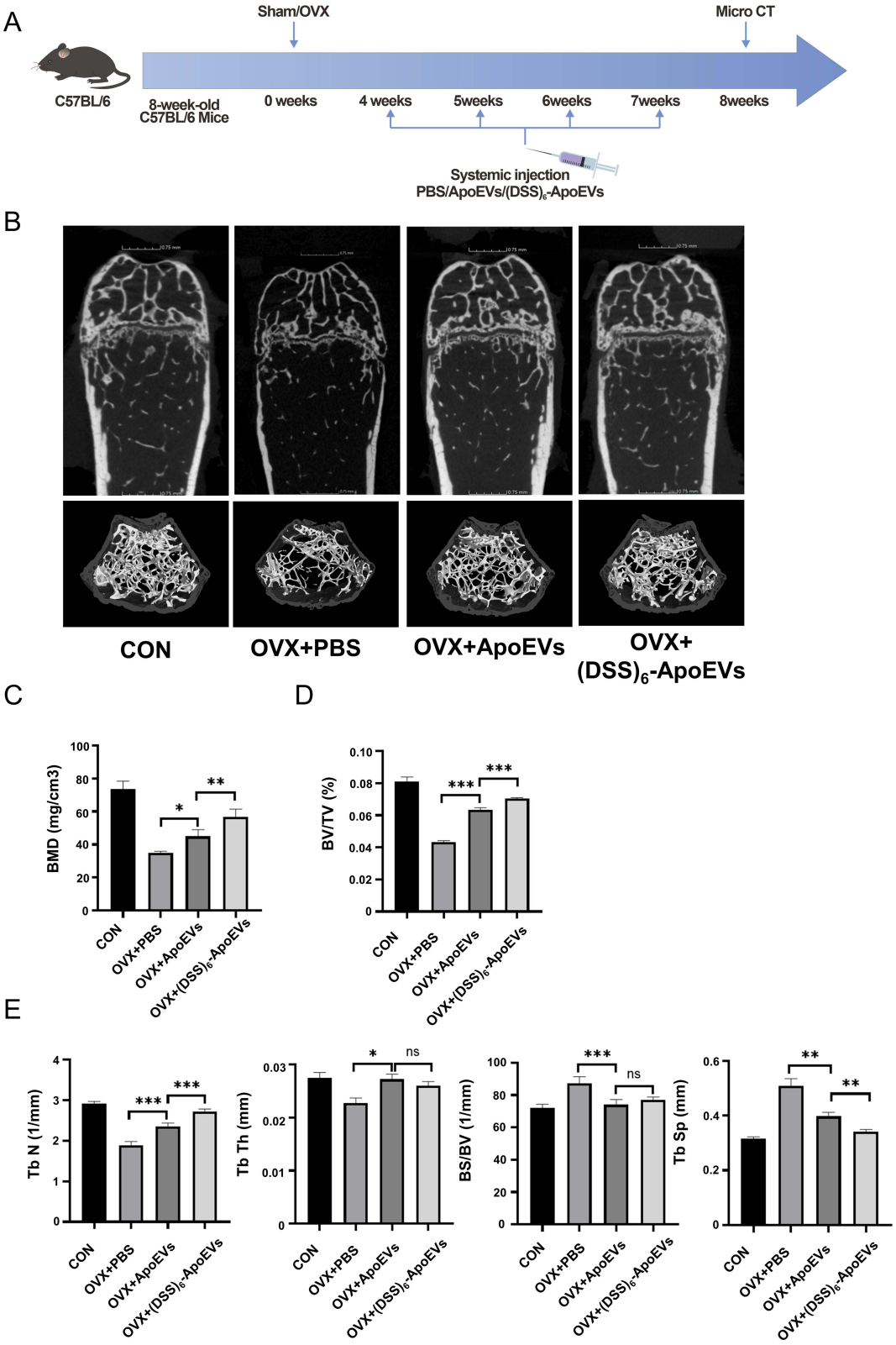

Figure 5 Evaluation of antiosteoporosis efficacy of $(DSS)_6$-ApoEVs in vivo. (**A**) The therapeutic design of the $(DSS)_6$-ApoEVs. (**B**) Micro-CT 3D structure image of mice femora of PBS-treated, ApoEVs-treated and $(DSS)_6$-ApoEVs-treated groups, compared with the control group. Scale bar, 0.75 mm. (**C**) BMD in distal femora were obtained from micro-CT analysis. (**D**) BV/TV in distal femora were obtained from micro-CT analysis. (**E**) Tb. N, Tb. Th, BS/BV, Tb. Sp in distal femora were obtained from micro-CT analysis. (n = 4). *P < 0.05, **P < 0.01, ***P< 0.001.

Abbreviations: NS, no significant; BMD, bone mineral density; BV, bone volume; TV, total volume; Tb. N, bone trabeculae number; Tb. Th, trabecular thickness; BS, bone surface; Tb. Sp, trabecular space.

(Figure S2). The expression of RNF146 reached its peak between 36 h and 48 h after adenovirus transduction (Figure 6A). After adenovirus transduction, BMSCs overexpressing RNF146 showed a better osteogenic differentiation capacity (Figure 6B and C). A green EGFP fluorescence signal was also found in ApoEVs induced after transduction, confirming that RNF146-overexpressed ApoEVs could be obtained using this method (Figure 6D). After loading RNF146 into the vesicles and further modifying with $(DSS)_6$, particle size was detected by DLS. Compared to ApoEVs and $(DSS)_6$-ApoEVs, the size of $ApoEVs^{RNF146}$ increased slightly after loading with RNF146, with an average diameter of 295–396 nm. The size of $(DSS)_6$-$ApoEVs^{RNF146}$ did not change significantly, with an average diameter of 295–396 nm (Figure 6E).

Furthermore, we performed in vitro experiments on drug-carrying vesicles. After 24 h of co-culture with BMSCs, most of the ApoEVs carrying upregulated RNF146 were ingested by cells and gathered around the nucleus (Figure 6F). ALP and Alizarin red staining showed that $ApoEVs^{RNF146}$ facilitated the osteogenesis of BMSCs (Figure 6G and H). These results indicate that transducing BMSCs with an adenovirus carrying the target gene and inducing apoptosis enables the generation of ApoEVs that overexpress the target proteins. RNF146 delivered by BMSCs-derived ApoEVs promotes osteogenic differentiation of BMSCs.

Anti-Osteoporotic Effects of $(DSS)_6$-$ApoEVs^{RNF146}$ In vivo

To investigate whether modification of the content packaged in ApoEVs can further enhance its osteogenic function, $(DSS)_6$-$ApoEVs^{RNF146}$ was established and administered to OVX mice via tail vein injection (Figure 7A). Micro-CT results showed that $(DSS)_6$-$ApoEVs^{RNF146}$ increased bone mass in OVX mice compared to that in the $(DSS)_6$-ApoEVs group (Figure 7B). Although we found that engineered ApoEVs with bone-targeting function significantly promoted BMD and BV/TV index, further loading of RNF146 to ApoEVs with bone-targeting function only promoted BMD index (Figure 7C and D). In addition, there were no significant differences between the DSS-$ApoEVs^{RNF146}$ and DSS-ApoEVs groups in terms of the micro-indicators of bone structures, such as Tb. N, BS/BV, and Tb. Sp (Figure 7E). These unexpected findings indicated that improving the bone-targeting function of ApoEVs might be more effective in alleviating osteoporosis than merely enhancing the biological function of ApoEVs.

Discussion

The current methods used for the treatment of osteoporosis possess inherent limitations, including the potential adverse effects of MRONJ and gastrointestinal dysfunction.[23–25] MSCs derived ApoEVs have demonstrated promising osteogenic capabilities, thus offering a novel avenue for the treatment of osteoporosis.[18,19] However, the clinical translation still faces significant challenges that natural ApoEVs are prone to be eliminated by phagocytic cells such as macrophages in the liver or spleen during blood circulation.[26–28] Consequently, the quantity of ApoEVs that ultimately reaches the desired target site is significantly diminished compared to the initial dosage, which would diminish the therapeutic effects of natural ApoEVs. Therefore, the development of engineered ApoEVs with a bone-targeting function holds great potential in augmenting the therapeutic efficacy of natural ApoEVs.

The strategic coupling of bone-affinity molecules onto natural vesicles significantly enhances these vesicles' capacity for bone targeting. Currently, bisphosphonates (BPs), tetracyclines (TCs), and oligopeptides are three stable types of bone-targeting molecules known to exhibit bone-targeting effects.[29] BPs, due to their inherent affinity for bone and regulatory role in bone mineralization, are considered the primary therapeutic option for osteoporosis.[30–32] However, employing BPs as a bone-targeting component can potentially lead to complications, such as atypical femur fractures, mandibular osteonecrosis, and extraneous skeletal adverse reactions.[23,24,33] TCs, capable of chelating with Ca^{2+} in hydroxyapatite,[34,35] exhibit not only bone-targeting properties but also inhibit collagenase,[36] thereby minimizing bone resorption. Despite these advantages, TCs usage may result in side-effects like rashes, dizziness, and nausea.[37] Acidic oligopeptides, comprising repeating aspartic acid or glutamic acid, can also function as a bone-targeting mechanism, since these recurrent acidic amino acids—present in native bone proteins—can interact with Ca^{2+} in mineralized tissues.[38]

In our research, we specifically selected a peptide with a repeat sequence of Asp-Ser-Ser due to its strong binding affinity towards hydroxyapatite. This peptide structure bears resemblance to the unique Asp-Ser repeat sequence found in

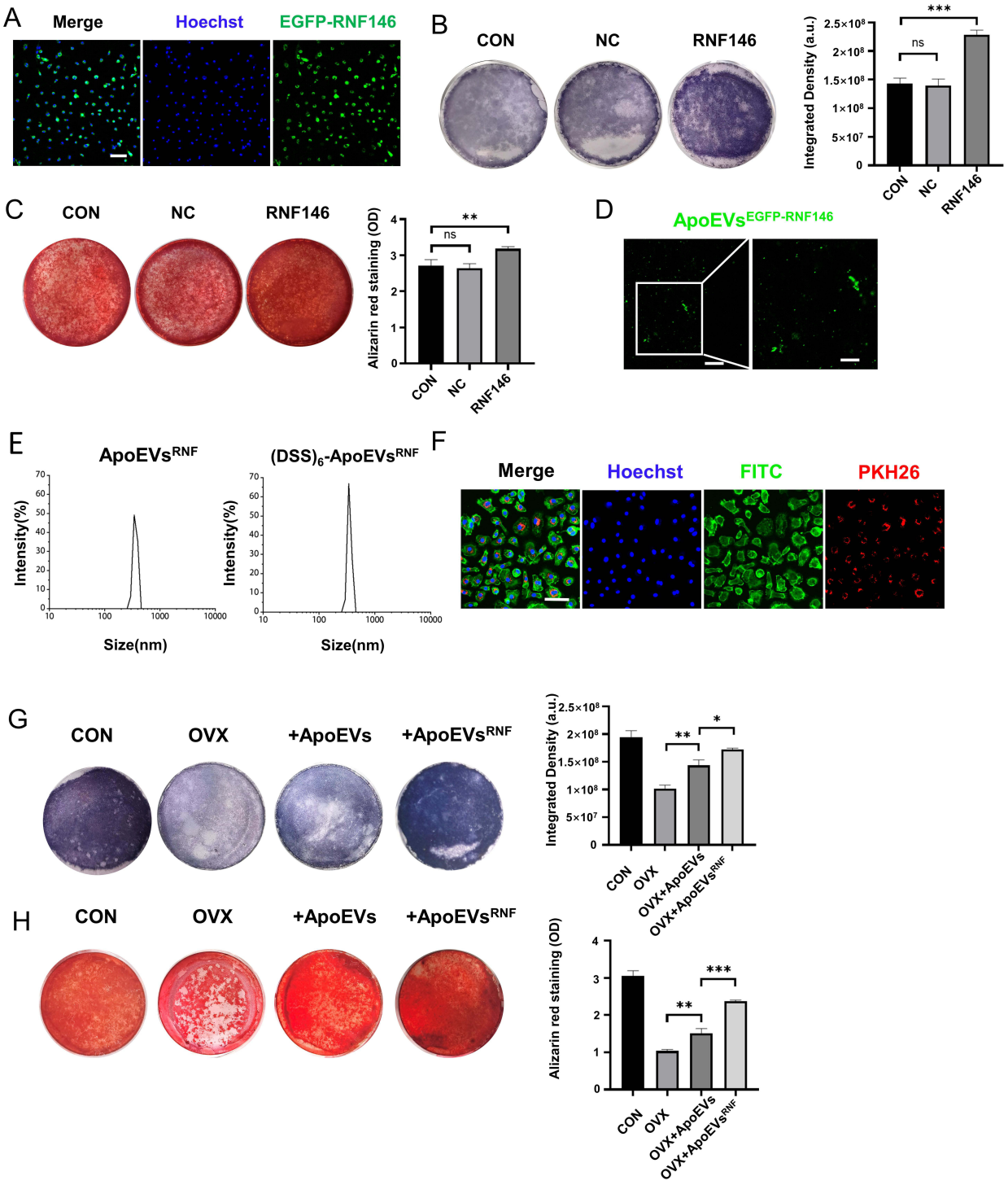

Figure 6 Osteogenesis promoting function of ApoEVs ^{RNF146} in vitro. (**A**) Representative images of the expression of RNF146 in BMSCs (P2) after transduction with HBAD-EGFP adenovirus for 36–48 hours observed by CLSM. Green, reporter gene EGFP carried by the adenovirus; blue, Hoechst labeled nucleus. Scale bar, 100 μm. (**B**) ALP staining showing the ALP activity of BMSCs transduced with adenovirus overexpressing RNF146 after osteogenic induction for 7 days. Quantitative analysis was performed using ImageJ software (n = 3). (**C**) Alizarin red staining of calcium nodules showing mineralized nodule formation in BMSCs transduced with an adenovirus overexpressing RNF146 after osteogenic induction for 28 days. Quantitative analysis was conducted by measuring absorbance at 540 nm (n = 3). (**D**) Representative images of ApoEVs induced by transduced BMSCs. Green: EGFP carried by RNF146. Scale bars: 20 (left) and 10 μm (right). (**E**) Size distribution of ApoEVs^{RNF146} and $(DSS)_6$-ApoEVs^{RNF146} analyzed by DLS. (**F**) Representative images of ApoEVs carrying upregulated RNF146 taken up by BMSCs, as observed using CLSM. Red, PKH26 labeled ApoEVs^{RNF146}; green, phalloidin-labeled cytoskeleton; blue, Hoechst labeled nucleus. Scale bar, 50 μm. (**G**) ALP staining showing ALP activity of BMSCs treated with ApoEVs and ApoEVs^{RNF146} after osteogenic induction for 7 days compared with the control group. Quantitative analysis was performed using ImageJ software (n = 3). (**H**) Alizarin red staining of calcium nodules showing mineralized nodule formation in BMSCs treated with ApoEVs and ApoEVs^{RNF146} after osteogenic induction for 28 days. Quantitative analysis was conducted by measuring absorbance at 540 nm (n = 3). *P < 0.05, **P < 0.01, ***P< 0.001.

Abbreviation: NS, no significant.

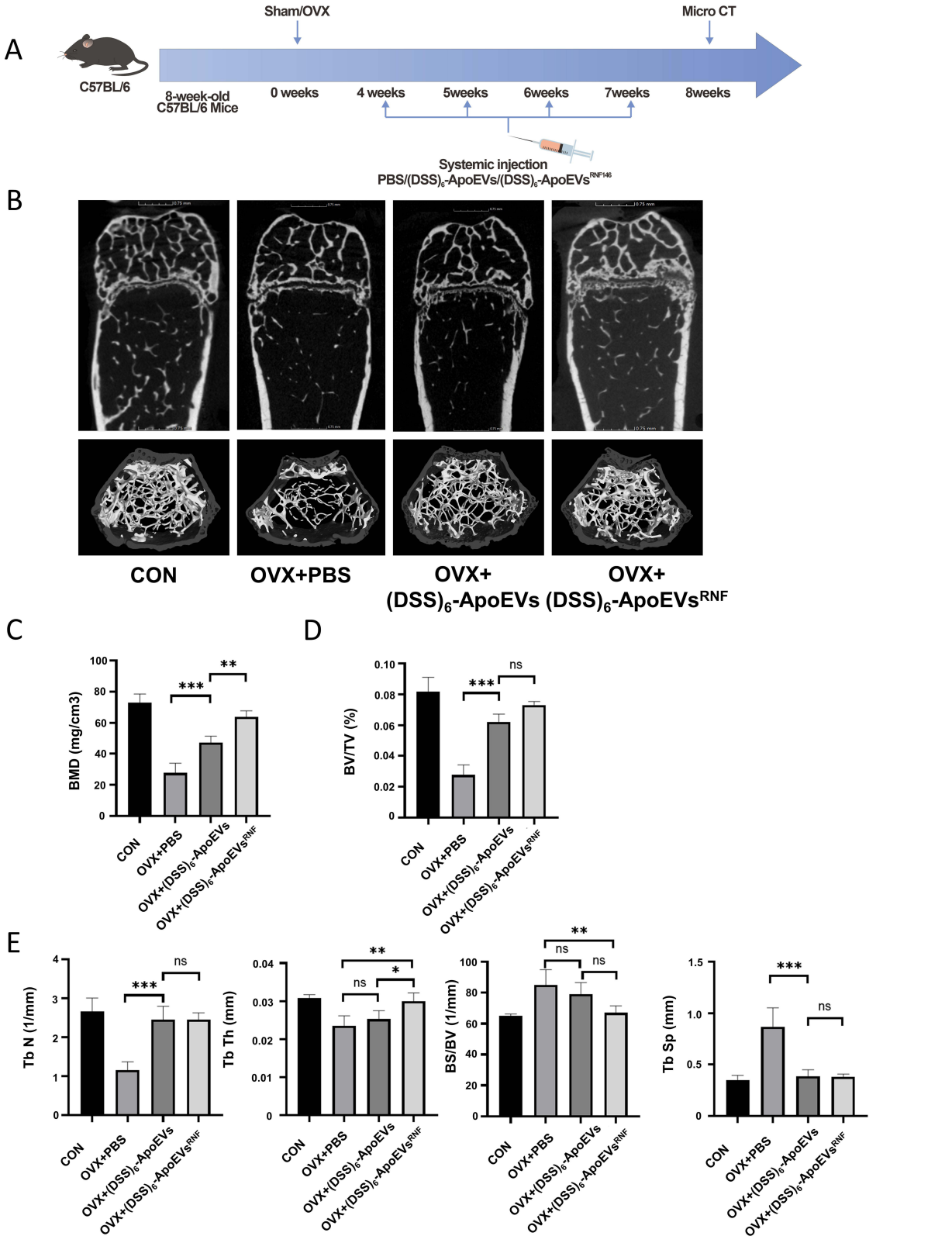

Figure 7 Evaluation of antiosteoporosis efficacy of $(DSS)_6$-ApoEVs^{RNF146} in vivo. (**A**) The therapeutic design of the $(DSS)_6$-ApoEVs^{RNF146}. (**B**) Micro-CT 3D structure image of mice femora of PBS-treated, $(DSS)_6$-ApoEVs-treated and $(DSS)_6$-ApoEVs^{RNF146}-treated groups, compared with the control group. Scale bar, 0.75 mm. (**C**) BMD in distal femora were obtained from micro-CT analysis. (**D**) BV/TV in distal femora were obtained from micro-CT analysis. (**E**) Tb. N, Tb. Th, BS/BV, Tb. Sp in distal femora were obtained from micro-CT analysis. n = 4. *P < 0.05, **P < 0.01, ***P< 0.001.

Abbreviations: NS, no significant; BMD, bone mineral density; BV, bone volume; TV, total volume; Tb. N, bone trabeculae number; Tb. Th, trabecular thickness; BS, bone surface; Tb. Sp, trabecular space.

dentin phosphoproteins, thereby inherently facilitating cellular uptake and internalization by various cell types. Furthermore, it demonstrates a simplistic spatial configuration, diminished immunogenicity, appreciable biocompatibility, and effortless modification.[39–43] These beneficial attributes render them exceptionally appropriate for in vivo applications. In addition, functionalized poly (ethylene glycol) (PEG) derivatives, such as pegylated phospholipids, which have been shown to greatly enhance the blood circulation time and stability of capsules, consequently reducing the elimination by the phagocytes in liver and spleen.[44,45]

In our research, DSPE-PEG-COOH was employed as a linker for the synthesis of $(DSS)_6$-ApoEVs. The stable amide linkage facilitated the attachment of $(DSS)_6$ onto the surface of ApoEVs without altering their size and morphology. This modification effectively eliminated the need for ligand modification, thereby reducing the risk of denaturation and loss of specific activity. The feasibility of the reaction was verified through HRMS and FTIR, while FC and CLSM analyses confirmed the binding of the peptide to the membrane surface of ApoEVs. DLS and TEM results indicated that $(DSS)_6$-ApoEVs closely resembled natural ApoEVs in terms of diameter and morphology. Furthermore, in vivo studies using frozen fluorescent sections of femur under CLSM and fluorescence imaging system demonstrated a significant enhancement in the bone-targeting capability of $(DSS)_6$, consequently improving bone formation. Moreover, $(DSS)_6$-ApoEVs exhibited improved microstructural indicators of bone tissue, such as BMD, BV/TV, Tb. N and BS/BV, compared to natural ApoEVs, thus proving their superior therapeutic effects. In vitro studies showed that BMSCs treated with $(DSS)_6$-ApoEVs exhibited increased osteogenic differentiation ability, as evidenced by intensified staining of ALP and alizarin red, along with elevated expression of osteogenesis-related proteins including ALP and RUNX2. Additionally, histological and serological analysis revealed no evidence of increased toxicity associated with $(DSS)_6$-ApoEVs.

ApoEVs can modulate the functions of other cells through three primary mechanisms. Predominantly, ApoEVs are phagocytosed by other cells and subsequently exert their biological effects through their unique contents. Prior research demonstrated that upon being phagocytosed and internalized by macrophages, ApoEVs inhibit the polarization of these cells towards a pro-inflammatory phenotype via the AMPK/SIRT1/NF-κB pathway.[22] Another study reported that ApoEVs delivered mitochondrial Tu translation elongation factor (TUFM) to endothelial cells, leading to an increase in autophagy levels, thus promoting angiogenesis and dental pulp regeneration.[21] The second functional mechanism of ApoEVs involves using signaling molecules on their vesicle membranes to act through ligand-receptor interactions. For instance, previous research found that calreticulin (CRT) exposed on the surface of ApoEVs acted as a critical "eat-me" signal mediating macrophage efferocytosis, which could alleviate type 2 diabetes (T2D) by inducing macrophage reprogramming.[46] The third functional mechanism of ApoEVs entails releasing metabolites through specific protein channels such as Pannexin 1. A study, for example, reported that ApoEVs can promote muscle regeneration by releasing creatine via the activated Pannexin 1 channel during the myoblast fusion process.[47] Thus, to further enhance the osteogenic function of natural ApoEVs, we adopted the classical approach that ApoEVs employ to exert their function, which entails incorporating osteogenesis-promoting molecules into the cargo of ApoEVs. RNF146, an E3 ubiquitin ligase with a ring domain, mediates Axin degradation, consequently activating the Wnt/β-catenin pathway to facilitate osteogenesis.[48] Therefore, integrating RNF146 into natural ApoEVs might augment their osteogenic potential.

Presently, there are two methods for drug loading into EVs. One approach, known as exogenous (or post-secretion) loading, involves loading drugs into EVs after their secretion from cells. This technique is typically achieved through extrusion, electroporation, ultrasound, and freeze-thaw processes. The second method, referred to as endogenous (or pre-secretion) loading, introduces drugs into cells before EVs secretion, resulting in the generation of drug-encapsulating EVs.[49] In our study, we employed a pre-secretory loading strategy to introduce drugs into cells via targeted adenovirus transduction. Fluorescence imaging results indicated successful loading of RNF146 into ApoEVs, while DLS results confirmed that the diameter of RNF146-modified ApoEVs was similar to that of natural ApoEVs. Furthermore, osteogenic functionality experiments suggested that RNF146-modified ApoEVs could further enhance osteogenesis in vitro and alleviate osteoporosis in vivo.

In our study, we devised and synthesized engineered ApoEVs with enhanced functionalities. Our engineered extracellular vesicles exhibited the ability to target bone and stimulate bone formation. However, our study had certain limitations due to its small-scale nature. Further research is warranted to achieve large-scale in vitro synthesis of engineered ApoEVs. Additionally, our current comprehension of all the components within ApoEVs remains incomplete,

rendering them somewhat of a "black box". Therefore, further investigations are imperative to elucidate the constituents of ApoEVs more comprehensively.

Conclusion

In summary, in our efforts to enhance the bone-targeting capabilities of natural ApoEVs, we harnessed the bone-affinity Asp-Ser-Ser repeat sequence, denoted as $(DSS)_6$, to modify these vesicles. Our findings revealed that $(DSS)_6$-modified ApoEVs exhibited comparable physical and chemical characteristics while maintaining biological safety, akin to natural ApoEVs. Furthermore, these engineered $(DSS)_6$-ApoEVs displayed a heightened affinity for bone tissue and demonstrated a remarkable capacity to promote osteogenesis. This enhanced functionality significantly ameliorated osteoporosis compared to their natural counterparts. To further enhance the osteogenic potential of ApoEVs, we employed adenovirus transfection to introduce the Wnt/β-catenin pathway agonist, RNF146, into ApoEVs and finally synthesized $(DSS)_6$-$ApoEVs^{RNF146}$, which exhibited the ability to greatly stimulate osteogenesis in vitro and effectively mitigate osteoporosis in vivo. These findings hold promise for the future of osteoporosis treatment.

Author Contributions

All authors made a significant contribution to the work reported, whether that is in the conception, study design, execution, acquisition of data, analysis and interpretation, or in all these areas. All authors took part in drafting, revising or critically reviewing the article, and agree to be accountable for all aspects of the work.

Funding

This study was supported by the National Key Research and Development Program of China (2022YFA1104400 to Yan Jin) and The National Natural Science Foundation of China (81930025 to Yan Jin, 82202341 to Xiaoshan Yang).

Disclosure

The authors declare no competing interests in the reported work.

References

1. Lorentzon M. Treating osteoporosis to prevent fractures: current concepts and future developments. *J Intern Med*. 2019;285(4):381–394. doi:10.1111/joim.12873
2. Estell EG, Rosen CJ. Emerging insights into the comparative effectiveness of anabolic therapies for osteoporosis. *Nat Rev Endocrinol*. 2021;17(1):31–46. doi:10.1038/s41574-020-00426-5
3. Cummings SR, Melton LJ. Epidemiology and outcomes of osteoporotic fractures. *Lancet*. 2002;359(9319):1761–1767. doi:10.1016/s0140-6736(02)08657-9
4. Song S, Guo Y, Yang Y, Fu D. Advances in pathogenesis and therapeutic strategies for osteoporosis. *Pharmacol Ther*. 2022;237:108168. doi:10.1016/j.pharmthera.2022.108168
5. Sanchez A, Blanco R. Osteonecrosis of the jaw (ONJ) and atypical femoral fracture (AFF) in an osteoporotic patient chronically treated with bisphosphonates. *Osteoporos Int*. 2017;28(3):1145–1147. doi:10.1007/s00198-016-3840-z
6. Zhou X, Cornel EJ, Fan Z, He S, Du J. Bone-targeting polymer vesicles for effective therapy of osteoporosis. *Nano Lett*. 2021;21(19):7998–8007. doi:10.1021/acs.nanolett.1c02150
7. Khan M, Cheung AM, Khan AA. Drug-related adverse events of osteoporosis therapy. *Endocrinol Metab Clin North Am*. 2017;46(1):181–192. doi:10.1016/j.ecl.2016.09.009
8. Gambrell RD Jr. The menopause: benefits and risks of estrogen-progestogen replacement therapy. *Fertil Steril*. 1982;37(4):457–474. doi:10.1016/s0015-0282(16)46149-2
9. Xiao Y, Mareddy S, Crawford R. Clonal characterization of bone marrow derived stem cells and their application for bone regeneration. *Int J Oral Sci*. 2010;2(3):127–135. doi:10.4248/IJOS10045
10. Zimmermann CE, Gierloff M, Hedderich J, Acil Y, Wiltfang J, Terheyden H. Survival of transplanted rat bone marrow-derived osteogenic stem cells in vivo. *Tissue Eng Part A*. 2011;17(7–8):1147–1156. doi:10.1089/ten.TEA.2009.0577
11. Bergmann A, Steller H. Apoptosis, stem cells, and tissue regeneration. *Sci Signal*. 2010;3(145):re8. doi:10.1126/scisignal.3145re8
12. Ma L, Chen C, Liu D, et al. Apoptotic extracellular vesicles are metabolized regulators nurturing the skin and hair. *Bioact Mater*. 2023;19:626–641. doi:10.1016/j.bioactmat.2022.04.022
13. Liu M, Sun Y, Zhang Q. Emerging role of extracellular vesicles in bone remodeling. *J Dent Res*. 2018;97(8):859–868. doi:10.1177/0022034518764411
14. Poon IKH, Parkes MAF, Jiang L, et al. Moving beyond size and phosphatidylserine exposure: evidence for a diversity of apoptotic cell-derived extracellular vesicles in vitro. *J Extracell Vesicles*. 2019;8(1):1608786. doi:10.1080/20013078.2019.1608786
15. Tang H, Luo H, Zhang Z, Yang D. Mesenchymal stem cell-derived apoptotic bodies: biological functions and therapeutic potential. *Cells*. 2022;11(23):3879. doi:10.3390/cells11233879

16. Santavanond JP, Rutter SF, Atkin-Smith GK, Poon IKH. Apoptotic bodies: mechanism of formation, isolation and functional relevance. *Subcell Biochem*. 2021;97:61–88. doi:10.1007/978-3-030-67171-6_4
17. Caruso S, Poon IKH. Apoptotic cell-derived extracellular vesicles: more than just debris. *Front Immunol*. 2018;9:1486. doi:10.3389/fimmu.2018.01486
18. Liu D, Kou X, Chen C, et al. Circulating apoptotic bodies maintain mesenchymal stem cell homeostasis and ameliorate osteopenia via transferring multiple cellular factors. *Cell Res*. 2018;28(9):918–933. doi:10.1038/s41422-018-0070-2
19. Li M, Xing X, Huang H, et al. BMSC-derived ApoEVs promote craniofacial bone repair via ROS/JNK signaling. *J Dent Res*. 2022;101(6):714–723. doi:10.1177/00220345211068338
20. Alma Zernecke KB, Noels H, Shagdarsuren E, et al. Delivery of microRNA-126 by apoptotic bodies induces CXCL12-dependent vascular protection. *Sci Signal*. 2009;2(100):ra81.
21. Li Z, Wu M, Liu S, et al. Apoptotic vesicles activate autophagy in recipient cells to induce angiogenesis and dental pulp regeneration. *Mol Ther*. 2022;30(10):3193–3208. doi:10.1016/j.ymthe.2022.05.006
22. Ye Q, Xu H, Liu S, et al. Apoptotic extracellular vesicles alleviate Pg-LPS induced inflammatory responses of macrophages via AMPK/SIRT1/NF-kappaB pathway and inhibit osteoclast formation. *J Periodontol*. 2022;93(11):1738–1751. doi:10.1002/JPER.21-0657
23. Reyes C, Hitz M, Prieto-Alhambra D, Abrahamsen B. Risks and benefits of bisphosphonate therapies. *J Cell Biochem*. 2016;117(1):20–28. doi:10.1002/jcb.25266
24. Dell RM, Adams AL, Greene DF, et al. Incidence of atypical nontraumatic diaphyseal fractures of the femur. *J Bone Miner Res*. 2012;27(12):2544–2550. doi:10.1002/jbmr.1719
25. Hatzenbuehler J, Pulling TJ. Diagnosis and management of osteomyelitis. *Am Fam Physician*. 2011;84(9):1027–1033.
26. Wiklander OP, Nordin JZ, O'Loughlin A, et al. Extracellular vesicle in vivo biodistribution is determined by cell source, route of administration and targeting. *J Extracell Vesicles*. 2015;4:26316. doi:10.3402/jev.v4.26316
27. Yamashita T, Takahashi Y, Nishikawa M, Takakura Y. Effect of exosome isolation methods on physicochemical properties of exosomes and clearance of exosomes from the blood circulation. *Eur J Pharm Biopharm*. 2016;98:1–8. doi:10.1016/j.ejpb.2015.10.017
28. Parada N, Romero-Trujillo A, Georges N, Alcayaga-Miranda F. Camouflage strategies for therapeutic exosomes evasion from phagocytosis. *J Adv Res*. 2021;31:61–74. doi:10.1016/j.jare.2021.01.001
29. Shi C, Wu T, He Y, Zhang Y, Fu D. Recent advances in bone-targeted therapy. *Pharmacol Ther*. 2020;207:107473. doi:10.1016/j.pharmthera.2020.107473
30. Brown JP, Morin S, Leslie W, et al. Bisphosphonates for treatment of osteoporosis: expected benefits, potential harms, and drug holidays. *Cana Family Physician Med Famille Canadien*. 2014;60(4):324–333.
31. Drake MT, Clarke BL, Khosla S. Bisphosphonates: mechanism of action and role in clinical practice. *Mayo Clin Proc*. 2008;83(9):1032–1045. doi:10.4065/83.9.1032
32. Lawson MA, Xia Z, Barnett BL, et al. Differences between bisphosphonates in binding affinities for hydroxyapatite. *J Biomed Mater Res B Appl Biomater*. 2010;92(1):149–155. doi:10.1002/jbm.b.31500
33. Khan AA, Morrison A, Hanley DA, et al. Diagnosis and management of osteonecrosis of the jaw: a systematic review and international consensus. *J Bone Miner Res*. 2015;30(1):3–23. doi:10.1002/jbmr.2405
34. Albert A, Rees CW. Avidity of the tetracyclines for the cations of metals. *Nature*. 1956;177(4505):433–434. doi:10.1038/177433a0
35. Wang J, Hu J, Zhang S. Studies on the sorption of tetracycline onto clays and marine sediment from seawater. *J Colloid Interface Sci*. 2010;349(2):578–582. doi:10.1016/j.jcis.2010.04.081
36. Reichert JC, Cipitria A, Epari DR, et al. A tissue engineering solution for segmental defect regeneration in load-bearing long bones. *Sci Transl Med*. 2012;4(141):141ra93. doi:10.1126/scitranslmed.3003720
37. Valentín S, Morales A, Sánchez JL, Rivera A. Safety and efficacy of doxycycline in the treatment of rosacea. *Clin Cosmet Investig Dermatol*. 2009;2:129–140. doi:10.2147/ccid.s4296
38. Rotman SG, Grijpma DW, Richards RG, Moriarty TF, Eglin D, Guillaume O. Drug delivery systems functionalized with bone mineral seeking agents for bone targeted therapeutics. *J Control Release*. 2018;269:88–99. doi:10.1016/j.jconrel.2017.11.009
39. Zhang G, Guo B, Wu H, et al. A delivery system targeting bone formation surfaces to facilitate RNAi-based anabolic therapy. *Nat Med*. 2012;18(2):307–314. doi:10.1038/nm.2617
40. Yang YS, Xie J, Wang D, et al. Bone-targeting AAV-mediated silencing of Schnurri-3 prevents bone loss in osteoporosis. *Nat Commun*. 2019;10(1):2958. doi:10.1038/s41467-019-10809-6
41. Yang K, Miron RJ, Bian Z, Zhang YF. A bone-targeting drug-delivery system based on Semaphorin 3A gene therapy ameliorates bone loss in osteoporotic ovariectomized mice. *Bone*. 2018;114:40–49. doi:10.1016/j.bone.2018.06.003
42. Liang C, Guo B, Wu H, et al. Aptamer-functionalized lipid nanoparticles targeting osteoblasts as a novel RNA interference-based bone anabolic strategy. *Nat Med*. 2015;21(3):288–294. doi:10.1038/nm.3791
43. Ravindran S, Snee PT, Ramachandran A, George A. Acidic domain in dentin phosphophoryn facilitates cellular uptake: implications in targeted protein delivery. *J Biol Chem*. 2013;288(22):16098–16109. doi:10.1074/jbc.M113.450585
44. Jain S, Deore SV, Ghadi R, Chaudhari D, Kuche K, Katiyar SS. Tumor microenvironment responsive VEGF-antibody functionalized pH sensitive liposomes of docetaxel for augmented breast cancer therapy. *Mater Sci Eng C Mater Biol Appl*. 2021;121:111832. doi:10.1016/j.msec.2020.111832
45. Maruyama K, Takizawa T, Yuda T, Kennel SJ, Huang L, Iwatsuru M. Targetability of novel immunoliposomes modified with amphipathic poly(ethylene glycol)s conjugated at their distal terminals to monoclonal antibodies. *BBA*. 1995;1234(1):74–80. doi:10.1016/0005-2736(94)00263-o
46. Zheng C, Sui B, Zhang X, et al. Apoptotic vesicles restore liver macrophage homeostasis to counteract type 2 diabetes. *J Extracell Vesicles*. 2021;10(7):e12109. doi:10.1002/jev2.12109
47. Ye Q, Qiu X, Wang J, et al. MSCs-derived apoptotic extracellular vesicles promote muscle regeneration by inducing Pannexin 1 channel-dependent creatine release by myoblasts. *Int J Oral Sci*. 2023;15(1):7. doi:10.1038/s41368-022-00205-0
48. Zhang Y, Liu S, Mickanin C, et al. RNF146 is a poly (ADP-ribose)-directed E3 ligase that regulates axin degradation and Wnt signalling. *Nat Cell Biol*. 2011;13(5):623–629. doi:10.1038/ncb2222
49. Liao W, Du Y, Zhang C, et al. Exosomes: the next generation of endogenous nanomaterials for advanced drug delivery and therapy. *Acta Biomater*. 2019;86:1–14. doi:10.1016/j.actbio.2018.12.045